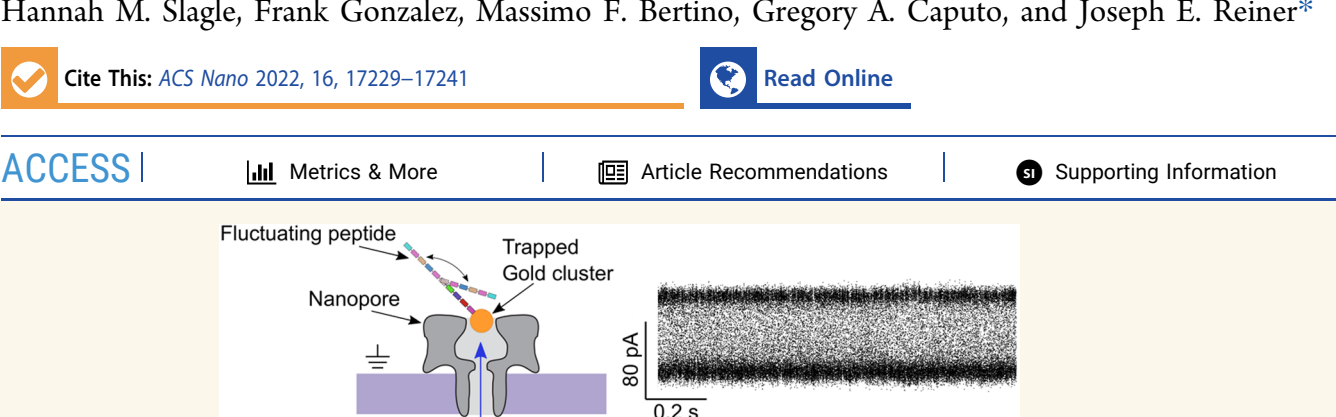
www.acsnano.org

Downloaded via NATL INST OF STANDARDS & TECHNOLOGY on June 12, 2023 at 22:56:15 (UTC). See https://pubs.acs.org/sharingguidelines for options on how to legitimately share published articles.

Selective Detection and Characterization of Small Cysteine-Containing Peptides with Cluster-Modified Nanopore Sensing

Madhav L. Ghimire, Bobby D. Cox, Cole A. Winn, Thomas W. Rockett, Nicholas P. Schifano, Hannah M. Slagle, Frank Gonzalez, Massimo F. Bertino, Gregory A. Caputo, and Joseph E. Reiner*



ABSTRACT: It was recently demonstrated that one can monitor ligand-induced structure fluctuations of individual thiolate-capped gold nanoclusters using resistive-pulse nanopore sensing. The magnitude of the fluctuations scales with the size of the capping ligand, and it was later shown one can observe ligand exchange in this nanopore setup. We expand on these results by exploring the different types of current fluctuations associated with peptide ligands attaching to tiopronin-capped gold nanoclusters. We show here that the fluctuations can be used to identify the attaching peptide through either the magnitude of the peptide-induced current jumps or the onset of high-frequency current fluctuations. Importantly, the peptide attachment process requires that the peptide contains a cysteine residue. This suggests that nanopore-based monitoring of peptide attachments with thiolate-capped clusters could provide a means for selective detection of cysteine-containing peptides. Finally, we demonstrate the cluster-based protocol with various peptide mixtures to show that one can identify more than one cysteine-containing peptide in a mixture.

KEYWORDS: nanocluster, nanopore, peptide, cysteine, biosensing, alpha hemolysin

Ionic current

eptide biomarkers are of great interest for biosensing applications given their ubiquitous role in the onset and development of various diseases. 1-3 The ability to monitor certain peptides from the peptidome could enable detection of cancer⁴⁻⁷ along with various inflammatory,⁸⁻¹⁰ neurodegenerative, 11-13 and cardiovascular diseases. 14-16 Several reviews have been written on the subject of peptide sensing for diagnostic and surveillance-based applications. 17,18 Given the vast number of different peptides that make up the peptidome (i.e., at least 4000 peptides have been reported in urine alone), 19 it is not surprising that most detection strategies have focused on various mass spectrometry (MS) methodologies. 20-22 The high degree of accuracy and precision provided by MS enables clear separation of different peptide components, but MS methods typically require labeling, show ca. 50% detection efficiency from tryptic digests, are nearly blind to cysteine-containing peptides, 23 and are not easily amenable to point-of-care analysis. In addition, MS analysis of proteins typically utilizes a trypsin digest that cleaves the protein sample into a large number of peptides. This can yield complex spectra that are cumbersome to analyze. One approach to overcome this is to utilize selective detection of cysteine to reduce the number of observable peptides. Cysteine detection is advantageous because of its tendency to bind to coinage metals and it is the rarest amino acid in the proteome. Selective detection of cysteine-containing peptides would greatly reduce the complexity of proteomic analysis, which motivates the development of rapid

Received: August 6, 2022 Accepted: September 27, 2022 Published: October 10, 2022





and low-cost methods for detecting small, cysteine-containing peptides in solution.

Non-MS-based peptide detection typically relies on immunoassay protocols where target antibodies can selectively detect peptides from a populated background. Several review articles describe this methodology in greater detail. ^{26–30} Despite the high degree of selectivity provided by immunoassays, they are limited by the difficulties in reproducible results and tedious sample preparation. ^{31,32} Peptide-based sensors have been proposed as well, and these show promise in their ability to selectively detect various targets from a crowded environment. ^{33–37} All these methods rely on the identification of a specific adapter to detect a particular peptide. Development of a transducer capable of selectively detecting a variety of molecules would represent a useful development in the field of peptide sensing. Several single molecule techniques have been applied to peptide detection, ^{38–40} but here we focus on resistive-pulse nanopore sensing.

Resistive-pulse nanopore sensing is a well-established singlemolecule technique with advantages that include label-free detection, low-cost implementation, and the ability to modify the sensor element for various detection strategies and applications. 41 The principle of operation is based on the Coulter counter where a nanosized hole in a membrane partition is used to detect single molecules that enter the hole and partially block the flow of current. These blockages can be analyzed to ascertain properties of the molecule in question. Recent efforts by nanopore researchers have focused on a variety of peptide and protein applications that include sequencing, 42-45 detection of various peptide modifications, 46,47 and peptide sensing and analysis. 48 Most efforts that apply nanopore detection to peptide sensing have utilized high-throughput detection to enable construction of size distributions, while fewer studies have used applications that utilize modifications to the nanopore environment to facilitate long-time extended interrogation of single molecules. 49,50 Some of these pore modification studies have the advantage of enabling clear identification of the molecule of interest without the need for constructing current blockade or transit time distributions. 51-55

Our group has previously utilized thiolate-capped metallic gold nanoclusters as a passive actuator capable of transmitting information about the structural dynamics of the particle. Further investigation showed that one can monitor ligand exchange processes at the single cluster limit. The introduction of free ligands in the vicinity of the pore-bound cluster yields easily resolved current transitions that correspond to the mass of the exchanging ligand. This suggests a path toward single molecule sensing and identification, which was demonstrated for the case of the tripeptide glutathione. S1

To fully develop this technique as a viable peptide sensor, more effort is required to better understand what types of fluctuations occur upon peptide attachment with the cluster. While the initial demonstration of ligand exchange showed promise, via the onset of distinguishable current steps for identifying the attaching ligands, it is not clear how universal these steps will be and what characteristics about the attaching peptide dictate the onset of clear current step fluctuations. Specifically, which chemical and physical properties of the peptides are most responsible for causing the different types of fluctuations upon ligand attachment? This motivates the present study and will serve as a major focus of this paper.

In the work presented herein, we explore the different fluctuations that result from attaching peptides to tiopronin (TP)-capped gold clusters. We investigate a range of peptide fluctuations that give rise to either well-resolved transitions between current states or high frequency, two-state fluctuations. We show that these high-frequency fluctuations result from a combination of peptide charge, sequence, and length. We also demonstrate improved peptide sensing results from these high-frequency fluctuations because they create distinct current signatures that enable peptide identification at the single peptide limit. Additionally, we find that peptide attachment requires a cysteine residue in the free peptide. Finally, we demonstrate clear identification of peptides from various mixtures, which provides a path toward cysteine selective, low molecular weight, peptide detection.

RESULTS AND DISCUSSION

Nanopore analysis can be used in conjunction with microcapillary tips to load individual metallic clusters into a pore. 56,57 This has been used to study ligand exchange processes on metallic clusters, 51 and we use this methodology here to further explore peptide induced current fluctuations. Figure 1 illustrates the experimental setup and typical traces that demonstrate peptide attachment. The sensor consists of a wild-type alpha hemolysin (α HL) pore, which is a stable, transmembrane, heptameric pore-forming toxin from Staphylococcus aureus. This αHL pore is loaded with a single TPcapped gold cluster locally injected into the cis-side of the pore. Single particle capture is most likely (rather than multiple particle capture) because the TP ligands are fully deprotonated in the pH 8 condition studied throughout, which makes the clusters charged and prone to cluster-cluster repulsion. Further discussion of this point can be found in the Methods section and elsewhere.⁵¹ Upon capture of a single cluster, pressure applied to the microcapillary containing clusters is turned off to further reduce the likelihood of multiple cluster captures. After a short delay (ca. seconds), solution from a second capillary, containing peptide ligands, is ejected onto the pore and this yields peptide attachment events. Detailed information regarding peptide sequence, charge and mass (Table S1) and CD spectra (Figure S1) highlighting the lack of any secondary structure in the peptides used in this study, can be found in the Supporting Information. Additionally, details regarding the size distribution of the gold clusters, the corresponding current blockades that result from cluster interactions with the pore, and UV-vis spectra of the clusters can be found in the Analysis of TP-Capped Nanoclusters section of the Supporting Information (Figures S2 and S3).

To facilitate the design of a cluster-modified nanopore peptide sensor, we experimented with numerous cysteine-containing model peptides varying the mass, primary sequence, charge, and terminal capping group to better understand the types of fluctuations that result from peptide-cluster interactions. Previous studies showed that when glutathione and thiolated polyethylene glycol (S-PEG) ligands undergo exchange and/or additions with TP-capped clusters, they give rise to easily resolved current steps that can be used to estimate the mass of the attaching ligand. Note that herein we use the term "attachment" to describe either a peptide exchange event or direct addition to the pore-bound cluster surface. See Figure 4 in ref 51 for a more complete discussion of the differences between ligand exchange and ligand additions. Interestingly, we find that attachment only works

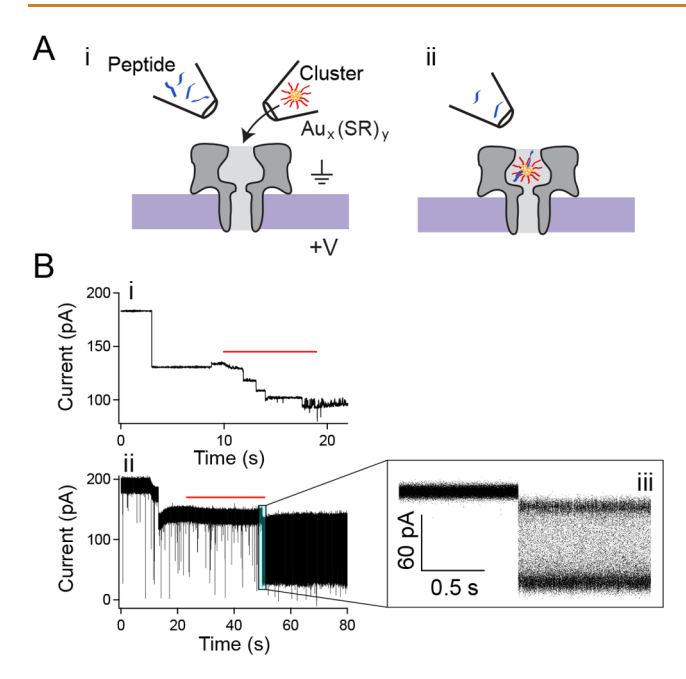


Figure 1. Experimental setup and corresponding peptide attachment traces. (A) Peptide attachment methodology with nanoporebased cluster analysis. (i) A single cluster is loaded into the pore and reduces the current. (ii) Following cluster capture, the target peptide is sprayed onto the trapped cluster and attachment occurs changing the corresponding ligand dynamics. (B) Sample traces illustrate two distinct fluctuation types. (i) A so-called lowfrequency fluctuation where several peptides lead to easily discernible current states. (ii) A high-frequency fluctuation where a single peptide yields rapid fluctuations. (iii) A zoomedin view of the resulting ligand dynamics exhibits two-state fluctuations that can be analyzed to identify the target peptide. The red bar in panels (i) and (ii) indicates when the peptide target is ejecting onto the pore. The narrow blue box around t = 50 s in (ii) highlights the zoomed region in (iii). All data shown here were taken under 70 mV applied transmembrane potential in 3 M KCl at pH 8. The "low-frequency" peptide in panel (B, (i)) is GRGDSPC at 500 µM in the loading tip, and the "high-frequency" peptide in panel (B, (ii)) is 9C1 at 250 µM in the loading tip.

for thiol-containing ligands. Consequentially, we find for the case of peptide ligands, they must contain a cysteine residue in order to initiate the attachment process. This is illustrated by numerous current traces comparing attachment (or lack thereof) for cysteine and noncysteine containing peptides (see Figure S4 in the Cysteine Selective Detection section of the Supporting Information).

In this study we find evidence of current stepwise transitions for some peptides (i.e., Figure 1B,i), but we also find a different type of interaction where the attachment of a peptide ligand yields high-frequency one- or two-state fluctuations (Figure 1B,ii,iii). A complete summary of which peptides give rise to which current fluctuations is included in Table S1 of the Supporting Information. We start with a series of experiments to better understand the underlying mechanisms that give rise to the so-called high-frequency current fluctuations.

The first experiment, highlighted in Figure 2, explores the dependence between the high-frequency two-state fluctuations and peptide size. We quantify differences between the peptides by measuring the difference between the TP-capped cluster level and the upper current state (defined as $\delta = i_{\rm TP} - i_{\rm upper}$) and the difference between the upper and lower current states

(defined as $\gamma = i_{upper} - i_{lower}$). We also find a clear dependence between peptide size and relative occupation of the lower or deeper current state. This is parametrized herein as $P_{\text{left}} = A_1/$ $(A_1 + A_2)$, where A_1 and A_2 are the heights of the two peaks in the all-points histograms for the peptide occupied current fluctuations (see Figure 2 for details). Figure 2 shows a dependence between the attaching peptide mass and δ , γ , and P_{left} . This dependence is expected for δ and γ because the difference between the TP-capped cluster before and after the attachment of a single peptide should reduce the current (proportional to δ), and the transitions between the upper and lower current levels likely result from the attached peptide fluctuating near the cluster surface (proportional to γ). However, the dependence between mass and P_{left} is less obvious, but it most likely results from the fact that the larger peptides are more prone to blocking the current for longer periods. Regardless of the mechanism driving the P_{left} dependence, we find a clear linear trend over the range studied. Taken together, these results suggest that differences between current fluctuations could be used to elucidate the identity of an attaching peptide. However, it is not clear what peptide properties give rise to two-state versus one-state highfrequency fluctuations or low-frequency fluctuations. This uncertainty complicates the development of the clusteroccupied pore as a sensor. To address this, we performed a series of experiments to better understand the mechanisms behind the various high-frequency fluctuations.

Figure 3 shows the role that cysteine position, peptide charge, and capping functional group play on the highfrequency fluctuations. Figure 3A,B shows sample current traces and corresponding all-points histograms for four different peptides. Each peptide has nine amino acid residues, with the lone cysteine residue located at different positions within each sequence (i.e., 9C1, 9C3, 9C5, and 9C7, see Table S1 in the Supporting Information for more details). Moving the cysteine residue further from the N-terminus yields twostate current fluctuations with diminishing occupation of the deeper current state. We hypothesize that this behavior results from the interactions between the carboxyl group on the TP ligands and the C- or N- termini of the peptide. Specifically, we believe the attaching peptide tends to be in either one of two structural configurations. One corresponds to the peptide being stretched out away from the cluster (larger volume yielding the lower current state), which we will refer to here as the "extended state", and the other configuration corresponds to the peptide being more closely associated with the cluster surface (smaller volume yielding the upper current state). For simplicity, we will refer to this configuration as the "collapsed state". The amine-carboxyl interaction (N-C) is most likely attractive, while the carboxyl-carboxyl interaction (C-C) is most likely repulsive at pH 8.58 This means that when the peptide end farther from the cluster is a carboxyl group (i.e., 9C1 and 9C3), the repulsive C-C interaction dominates and leads to rapid and clear fluctuations between the two structural configurations. Conversely, when the peptide N-terminus extends further away from the cluster surface (i.e., 9C5 and 9C7), the more attractive N-C interaction and/or entropic component of the peptide's free energy tends to favor the collapsed state and this creates a smaller volume structure, which leads to greater occupation of the higher current state. This is illustrated with the cartoon below Figure 3A,B.

To further confirm this hypothesis, we modified the end functional group of a peptide and compared the corresponding

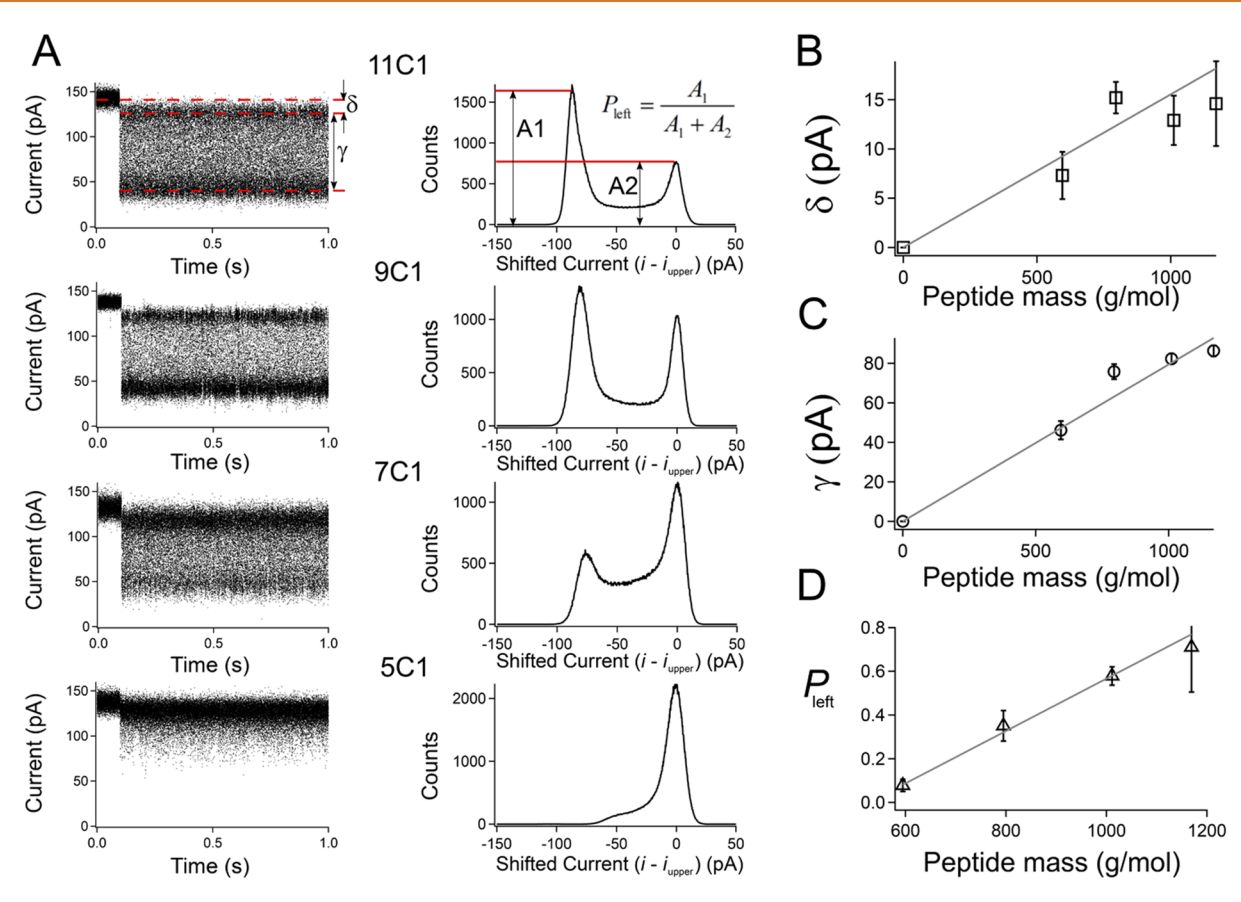


Figure 2. Size-dependent high-frequency peptide fluctuations. Peptides anchored at the N-terminus with a cysteine residue yield sizable current fluctuations. Peptides with different mass can be characterized by these fluctuations. (A) Sample current traces and ensemble-averaged all-points histograms for 11C1, 9C1, 7C1, and 5C1 (sequence information can be found in Table S1 of the Supporting Information) yield high-frequency fluctuations upon attachment of a single peptide at 0.1 s. Note that the steady current before capture results from a single trapped TP-capped Au cluster in the nanopore (see Figure 1). Also note the current distributions are shifted so the upper current state is positioned at zero. We parametrize the fluctuation magnitude with respect to the gold-occupied state (δ) and the magnitude of the fluctuations between the upper and lower peptide states (γ). The corresponding all-points histograms for each of the peptides show fluctuations yield two discrete states with the relative population of each state dictated by the peptide size. (B) A trend between the peptide mass and " δ " fluctuations exist. The solid gray line is a least-squares weighted-fit forced through the origin with slope (15.5 \pm 1.4) fA/(g/mol). (C) Additionally, a trend can be seen for " γ " fluctuations. The solid gray line is a least-squares weighted-fit forced through the origin with slope (79.4 \pm 1.6) fA/(g/mol). Note that both linear fits in parts (B) and (C) have been extended to the origin to illustrate the range of linearity. (D) The relative height of the left-most peak scales linearly with the peptide mass for all the peptides and suggests an additional metric (P_{left}) for peptide identification. The least-squares weighted fit yields a slope of (1.2 \pm 0.1) mmol/g. All data shown here were taken under 70 mV applied transmembrane potential in 3 M KCl at pH 8. The error bars are standard deviations calculated from a minimum of 6 different peptide capture events (details can be found in Table S2 of the Sup

current fluctuations. Figure 3C,D shows typical current traces and corresponding all-points histograms for both 7C1 and 7C1-NH₂ peptides. The 7C1-NH₂ peptides have the standard C-terminal carboxyl group modified with an amine capping group. The resulting traces show that the addition of the N-terminus-like moiety on the freely exposed end of the cluster-bound peptide nearly eliminates the lower current state. This is consistent with a model that claims the N–C interaction would lead to a more tightly bound peptide-cluster configuration, while the C–C interaction, expected for the 7C1 peptide, yields rapid transitions between the collapsed and extended state configurations. The cartoon below Figure 3C,D illustrates this behavior.

In addition to the role that the end functional group plays in driving these high-frequency fluctuations, we also hypothesize that charged residues can affect the two-state fluctuations as well. To confirm this, we performed measurements with positive, negative, and net-neutral versions of the 9C1 peptide.

Figure 3E,F shows current traces and histograms of these three peptides where the 9C1 negative peptide yields clearly resolved two-state fluctuations, while the net neutral and positive peptides essentially eliminate these fluctuations. We hypothesize that in this case, the charged residues interact with the deprotonated carboxyl residue of the TP ligands (measurements performed at pH 8), and this yields repulsive interactions for the negatively charged peptide and attractive interactions for the positive peptide. Once again the attractive interaction favors the collapsed state configuration, which leads to a single, higher-level current state for these peptide-particle pairs. The cartoon below Figure 3E,F illustrates this behavior.

The experiments outlined in Figures 2 and 3 lead to several conclusions regarding the high frequency fluctuations. First, longer peptides are more likely to exhibit two-state fluctuations. Second, the location of the cysteine residue with respect to the C- or N-terminus plays an important role in predicting the onset of two-state fluctuations. Specifically,

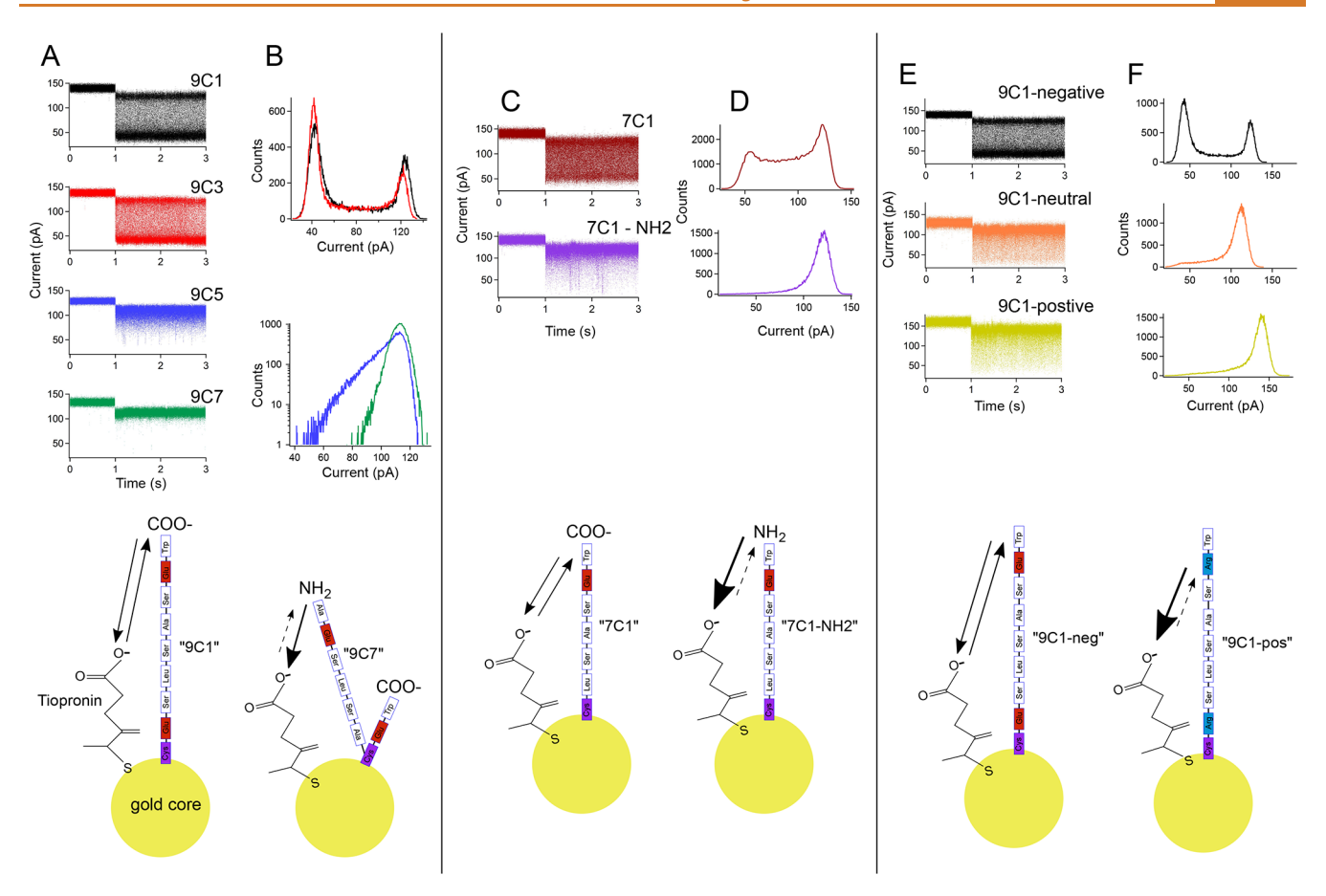


Figure 3. Fluctuations depend on the cysteine position, end functional group, and peptide charge. Each current trace shows a single TP-capped gold cluster trapped in the pore for 1 s. At t = 1 s, the corresponding peptide is attached to the cluster and various fluctuations ensue. These fluctuations inform about the nature of the peptide/particle interactions. (A, B) The cysteine location in the peptide anchors the peptide to the gold cluster and yields various fluctuations. For the 9C1 peptide, the carboxyl group is furthest away from the core, and this gives rise to well-resolved two-state fluctuations. As the cysteine is positioned near the carboxyl end, the amine group is free to interact with the TP ligands. This gives rise to a more stable and smaller configuration as evidenced by the fluctuations and corresponding all-points histograms. (C, D) Substituting the end functional group from carboxyl (7C1) to amine (7C1-NH₂) leads to a more stable and compact conformation. (E, F) Residue charge also affects the fluctuations as seen in the current traces. Negatively charged peptides tend to resist peptide coiling, which in turn yields clearly resolved two-state fluctuations. Net-neutral and positively charged peptides enable more compact cluster structures that eliminate the deeper current state. The cartoon models below each experimental set illustrate each of the stated hypotheses from the main text. Note that the all-points histograms correspond to the current traces shown. An ensemble of each peptide's histogram distributions along with averaged histograms can be found in Figure S5 of the Supporting Information. All data shown here were taken under 70 mV applied transmembrane potential in 3 M KCl at pH 8.

peptides having the cysteine near the N-terminus are more likely to yield two-state fluctuations. Third, the overall net charge of the peptide also plays a role in the onset of two-state fluctuations. Positive charges tend to create smaller and more stable clusters that eliminate the two-state fluctuations.

It is important to understand the mechanisms that drive these fluctuations because the goal here is to utilize peptide attachment with gold clusters to identify peptides. Given the complex nature of the induced fluctuations from peptide attachment, knowing the connections between peptide sequence and fluctuation type will help with the development of this protocol for peptide sensing. It is worth noting that we have assumed the observed fluctuations reported in Figure 3 result from interactions between the peptides and the carboxyl group of the TP. It is possible that there may be interactions with the nanopore as well. We believe this is less likely given the fact that the *cis*-side of the α HL pore has a roughly equal mixture of positive and negative residues, but we have not definitively ruled this out here. Utilizing mutated forms of the

 α HL pore or molecular dynamic simulations would be required to explore this question in greater detail, but that is beyond the scope of the present manuscript, and we leave this question to a future study.

We begin the sensor discussion by exploring peptide analysis of discrete current steps. Developing the cluster-nanopore sensor for detecting and identifying peptides from clearly resolved current steps requires a calibration curve relating current step size to peptide mass. Figure 4 shows a typical current trace for one such peptide (GRGDSPC). We believe this peptide gives rise to clear current steps as opposed to high-frequency two-state fluctuations because of the low mass and the location of the cysteine residue (see Figures 2 and 3A,B). This peptide yields clearly resolved current states that can be observed in the 100 Hz low-pass filtered signal (red trace overlapping the black trace in Figure 4A). An all-points histogram of the filtered signal (within the highlighted purple box) yields six well-resolved peaks that can be used to identify the different current levels associated with the attachment of

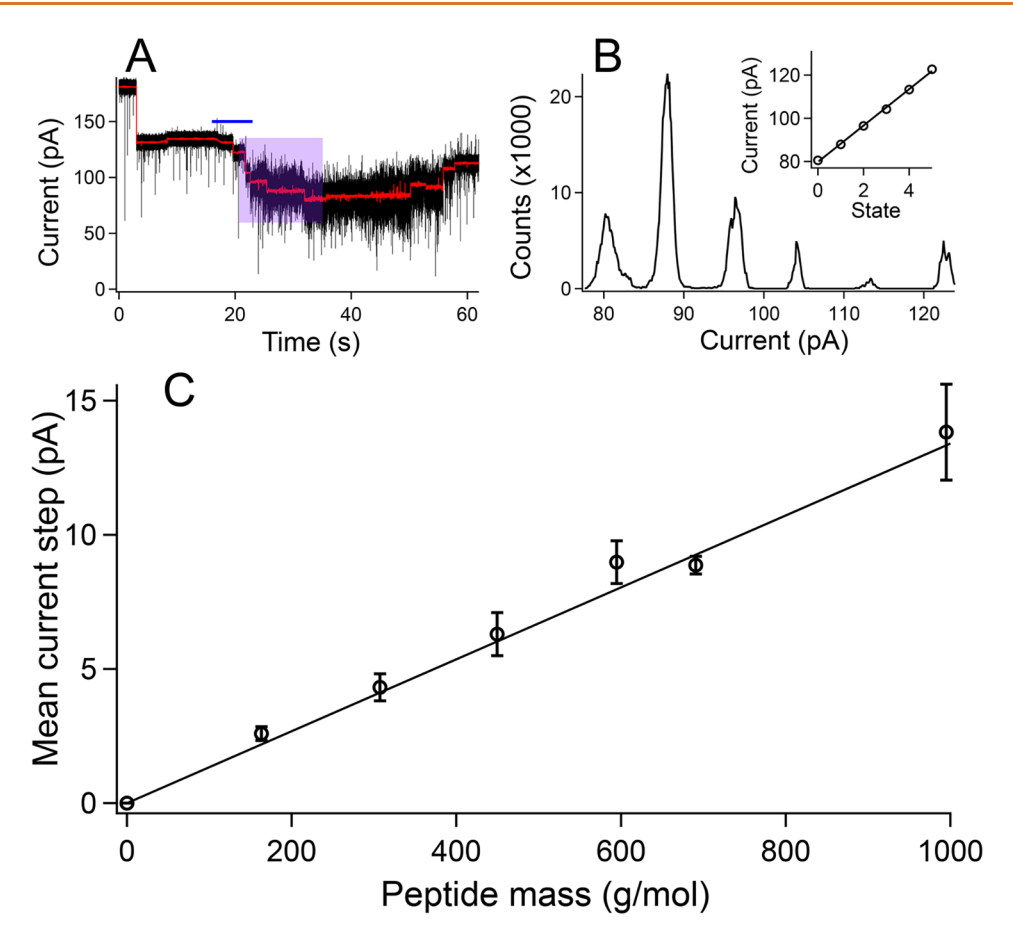


Figure 4. Step-based low-frequency peptide sensing. (A) Typical current trace of peptide attachments (this case shows GRGDSPC). The open pore current drops upon entry of a single TP-capped gold cluster at \approx 5s. Free peptide is ejected onto the pore from t=16 to 23 s as indicated with the blue bar. This yields clearly delineated steps in the current. The overlaid red trace shows the current filtered with a 100 Hz low-pass filter. (B) An all-points histogram of the attachment process (t=20-35 s, region highlighted with purple box) shows discrete current states. The inset shows the linearity of the peak positions, and the solid line is a least-squares fit whose slope is equal to the current step magnitude for that particular peptide. (C) The peak steps are nearly linear up to 1000 g/mol. The solid line is a least-squares fit with a slope value of (13.4 ± 0.4) fA/(g/mol), which is in reasonable agreement with the slope found in Figure 2B. The ligands and peptides shown here listed in order of increasing mass are (TP, glutathione, RGDC, 5C1, GRGDSPC, and 9C7). All data shown here were collected under 70 mV applied transmembrane potential in 3 M KCl pH 8 buffer. Sample current traces for each ligand can be found in the Supporting Information (Figure S6). Each data point corresponds to the average slope calculated from a minimum of 4 different cluster experiments. The error bars correspond to ± 1 SD.

this peptide (Figure 4B and inset). The slope of the inset plot in Figure 4B yields the current step magnitude for this peptide. We performed a similar step analysis for a variety of different peptides and ligands (see Figure S6 in the Current Step Ligand Analysis section of the Supporting Information for a complete summary), and Figure 4C shows the resulting linear dependence between the mean current step size and the ligand mass for these examples where the mass ranges between ca. 200 and 1000 g/mol.

The well-resolved current steps in Figure 4 suggest that it should be possible to identify peptides from a mixture. We illustrate proof-of-concept of this in Figure 5, which shows a sample current trace (100 Hz low-pass filtered) resulting from the ejection of a 1:1 mixture (500 μ M concentration in the pipet tips for each peptide) of RGDC and GRGDSPC peptides onto a nanopore-bound gold cluster. The ejection yields numerous current steps of various magnitude. We analyze the step magnitudes for the downward-going current transitions because those are the steps that most likely result from the attachment of another peptide onto the particle. Figure 5B shows the step-down distribution (black line and circles, Figure

5B) overlaid on the previously established RGDC (red) and GRGDSPC (blue) step transition distributions. The large peak centered at -6.8 pA nearly overlaps with the expected distribution from RGDC peptides, and we see a smaller number of events consistent with the GRGDSPC peptides centered at -9.7 pA. Clearly, the probability of attaching or exchanging a smaller peptide is greater than the larger peptide, which is not surprising given that the entropic penalty to bind a shorter peptide should be smaller. It is worth noting that the long times between current step transitions make peptide identification from a single current step straightforward. Figure 5C illustrates this point where eight stepdown transitions are labeled with colored numbers that correspond to the different peptides involved. The red numbers (steps 5, 6, and 8) most likely correspond to RGDC transitions, and the blue numbers (steps 2, 3, and 7) most likely correspond to GRGDSPC transitions. Steps 1 and 4 (black label) most likely correspond to a TP fluctuation. To quantify the likelihood of each step corresponding to a particular peptide, we performed a leastsquares fit using the RGDC and GRGDSPC distributions to the observed current step distribution. A complete description

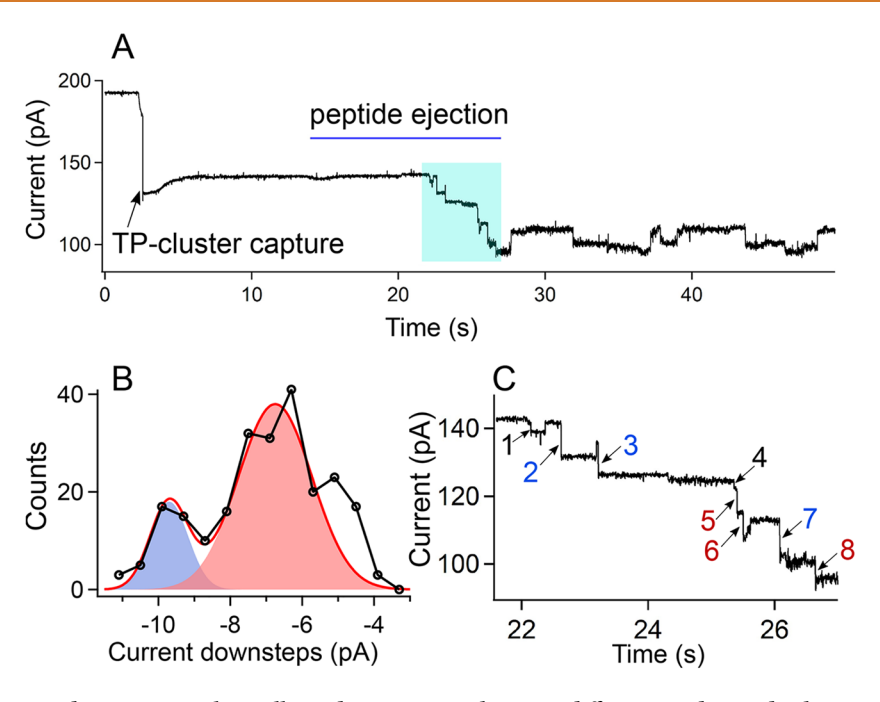


Figure 5. Low-frequency peptide mixture analysis allows discrimination between different-sized peptides by step-size comparison. (A) A typical current trace shows the capture of a TP-capped cluster at t = 2.6 s followed by continuous peptide spray onto the pore from t = 14 s-27 s (blue line). The signal is filtered at 100 Hz and a zoomed-in view of the sub region in blue from t = 22-27 s is shown in panel (C). (B) A distribution of 237 down steps (magnitude >4 pA) collected from 3 different experiments (24 clusters on 3 nanopores) superimposed on the corresponding distributions for each peptide individually (blue = GRGDSPC and red = RGDC). The distribution shows a greater frequency of RGDC fluctuations. The peak of each distribution is best fit to the mixture data (data = black circles, solid black line, fit = solid red line). (C) Clearly defined state transitions can be used to distinguish between the two peptides in the mixture. This shows a subset of the current trace (highlighted blue region in Figure 5A). Each number label in the trace corresponds to a peptide induced fluctuations with red numbers corresponding to RGDC, blue corresponding to GRGDSPC, and black to TP. Step 2 = 9.95 pA (GRGRDSPC with 98% probability), step 3 = 9.58 pA (GRGRDSPC 95%), step 5 = 7.24 pA (RGDC 99%), step 6 = 7.32 pA (RGDC 99%), step 7 = 12.06 pA (GRGDSPC 99%), and step 8 = 5.04 pA (RGDC 99%). Steps 1 and 4 are on the order of 2 pA and most likely correspond to TP fluctuations. Complete data analysis regarding the probability distributions can be found in the Methods section.

of the analysis can be found in the Nanopore Sensing and Data Analysis section.

Identifying the presence of various peptides from single capture events can also be extended to the high-frequency two-state fluctuating peptides because the addition of each peptide is separated by several seconds. Given the fact that many of the so-called high-frequency peptides exhibit distinct signatures in their corresponding current histograms (see Figures 2 and 3), it should be possible to identify a particular peptide in a mixture. Analyzing high-frequency peptides for sensing applications requires an understanding of how fluctuations behave with the addition of multiple peptides. In the low-frequency case (highlighted in Figures 4 and 5), the addition of more than one peptide does not complicate the fluctuations. The same does not hold for the high-frequency case. To address this, we present an example of peptide mixture detection for 7C1 and 9C1 peptides.

To begin, we show in Figure 6A,B how current fluctuations change with the addition of sequential 7C1 and 9C1 peptides onto a trapped cluster. To analyze these events, we filter the current signal with a 100 Hz low-pass filter. This allows one to clearly identify when another peptide attaches to the cluster (as evidenced by a downward step in the filtered current). Figure 6A shows the sequential addition of three 7C1 peptides on a single trapped cluster. The filtered data highlight each addition, and we calculate all-points histograms for each of the current states corresponding to the addition of another peptide. These distributions show a clear trend where the relative magnitude

of the lower current state (with respect to the upper current state) increases with each additional peptide. This is most effectively parametrized by P_{left} (see Figure 2).

We developed a simple model for $P_{\rm left}$ as a function of the number of peptides attached to the cluster. The model assumes the two-state current fluctuations are dependent on the peptides being in one of two conformations (see discussion connected to Figure 3 for more details). If we assume each peptide's conformation state is independent of all the other peptides on the cluster, then we can calculate the probability of finding the current in the deeper state, and this is directly related to $P_{\rm left}$. Complete details of this model are outlined in section 7 of the Supporting Information. Applying this model to the 7C1 data in Figure 6A shows reasonable agreement with the observed fluctuations (the model is represented by colored triangles and the data is black circles). Similar analysis is applied to the case of sequential 9C1 peptides attaching to the cluster. These results are highlighted in Figure 6B.

In Figure 6C, we present a typical current trace for a 7C1:9C1 mixture ejected onto a trapped cluster. In this case, we clearly identify four different states which we assume result from the addition of four peptides. Analyzing the $P_{\rm left}$ parameter for each state and comparing these results to our model shows that the first two states most likely correspond to the addition of two 7C1 peptides and the last two states most likely correspond to the addition of two 9C1 peptides. This is evidenced by the fact that the $P_{\rm left}$ data (black circles and line) are in better agreement with the 7C1 model additions (blue

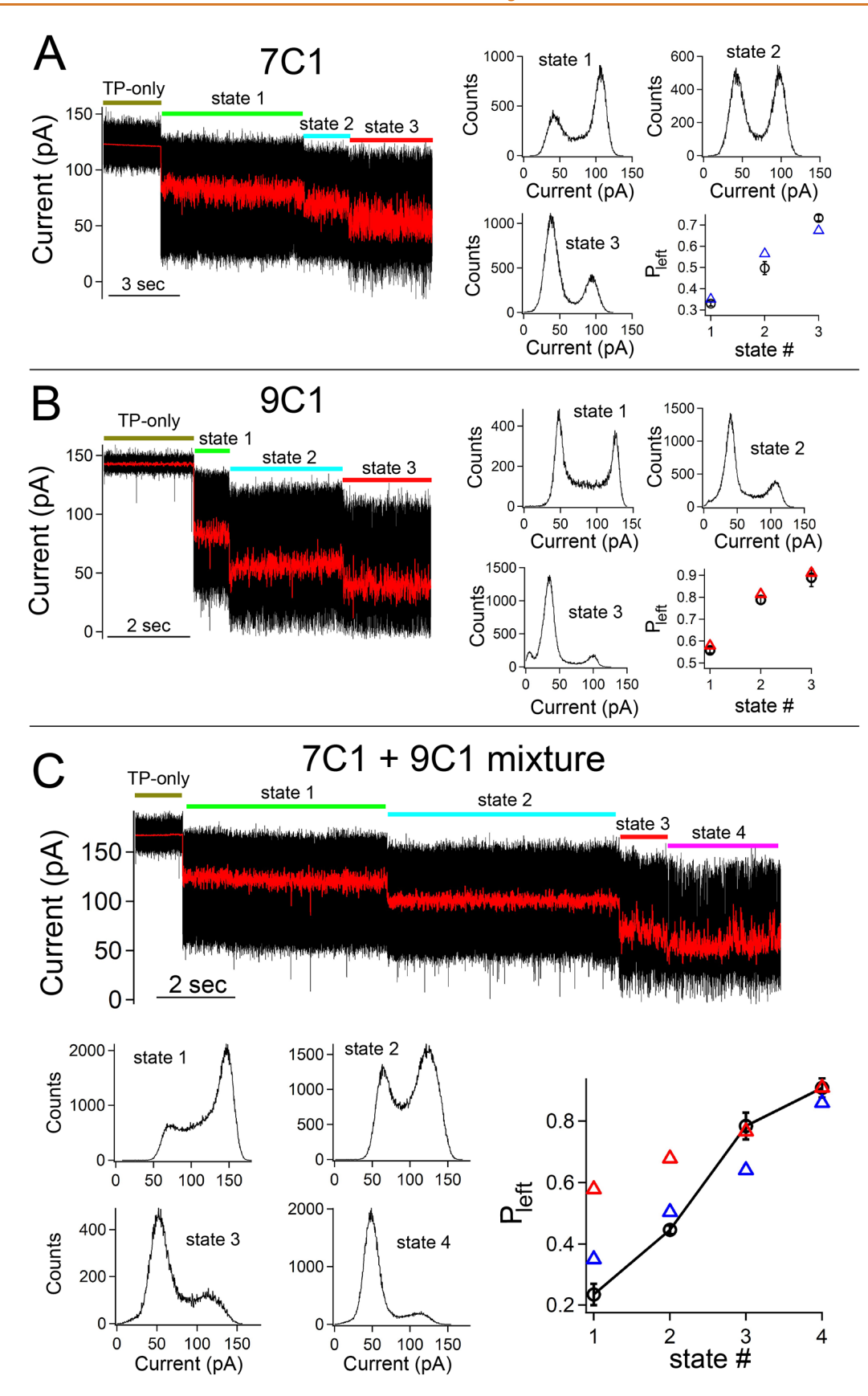


Figure 6. Multistep and mixture analysis for 7C1 and 9C1 peptides. Peptide addition can be clearly resolved with 100 Hz filtered steps (red traces) and corresponding histograms can be analyzed to identify attaching peptides. (A, left) Three consecutive 7C1 peptides attach to a single cluster giving rise to (A, right) distinct all-point current histograms. P_{left} data (black circles) (see Figure 2) shows reasonable agreement with a simple model (blue triangles) (see section 7 in the Supporting Information). (B) Similar behavior can be observed for 9C1 peptides where P_{left} data (black circles) show excellent agreement with a simplified model (red triangles). (C) A 1:3 molar mixture of 7C1

Figure 6. continued

and 9C1 peptides shows the addition of both peptide types on a single cluster. This particular current trace shows the addition of two 7C1 peptides, followed by two 9C1 peptides. This is verified in the P_{left} panel, where the blue triangles correspond to the addition of all 7C1 peptides and the red triangles correspond to the addition of 9C1 peptides. The data (black circles with solid line to guide the eye) overlap with the 7C1 model for peptides 1 and 2 and then agrees with the addition of 9C1 for peptides 3 and 4. Complete details are presented in Table S4 of the Supporting Information.

triangles) for states 1 and 2, and then the agreement is closer for 9C1 model additions (red triangles) for states 3 and 4. The overlap between the different peptides becomes difficult to resolve beyond state 3, which suggests that this $P_{\rm left}$ model analysis is limited to 2 or 3 peptides per cluster. Results from Figure 6 are summarized in Tables S3 and S4 of the Supporting Information.

Nanopore sensing with biological pores has been an active area of research for nearly 25 years. The technique provides a powerful analytical testbed with which to analyze unlabeled single molecule behavior in nanoconfined environments. Nanopore sensing has become increasingly focused on peptide detection in the past few years. 49 The cluster-based detection protocol outlined herein presents a number of advances for peptide detection. Cluster-based detection can selectively detect cysteine-containing peptides and remain blind to noncysteine containing peptides. This provides an advantage because a large percentage of peptides do not contain cysteine,⁵⁹ and this could serve as a selective tool to reduce the analytical complexity required to identify proteins from peptide fragments. While the cluster-based detection described herein may not yield distinct parameters for every peptide (see Figure 4 and Table S2 in the Supporting Information), it does give rise to very long-lived events (~seconds), which could be used to optimize peptide mixture analysis to identify peptides that give rise to distinct signatures. The advantage here is that the gold cluster approach yields additional parameters (e.g., P_{left}) beyond traditional open pore parameters (i.e., blockade depth, blockade time, etc.) that could be used to help identify a variety of cysteine containing peptides.

Cluster-based detection described here will most likely not enable *de novo* peptide sequencing, but the long-lived fluctuations (like those highlighted in Figures 3 and 6) should yield useful information to help identify some peptide characteristics. Specifically, whether or not one or more peptides in a mixture contains a cysteine, where is the cysteine most likely positioned (near the N- or C- terminus), what is the approximate size of the peptide, and if the peptide is charged or neutral. All of this information, coupled with protein digestion from several cleavage enzymes, ⁶⁰ could help identify a target peptide in a mixture.

Figure 6C shows that each cluster can only detect a small number of peptides before that cluster must be ejected from the pore (under a voltage polarity switch). This suggests single-pore cluster-based analysis may not be viable for analyzing relative peptide concentrations in mixtures. However, there has been considerable development of parallel nanopore systems (i.e., minION from ONT) that are capable of high throughput analysis (ca. 100s of individual nanopores), and we envision a similar setup could be used for our technique. Briefly, several microliters of gold clusters could be ejected with a pipet into the *cis*-side of the pore and microfluidic loading could be used to introduce and flush away peptide mixtures for continual analysis. The ability to apply independent voltages to a large number of nanopores would enable the application of voltage

reversals to nanopores containing clusters with too many peptides attached. This would enable the detection of large numbers of peptide fluctuations from which one could ascertain the relative concentration of the cysteine-containing peptides in a mixture.

Alternatively, cluster-based analysis with a single pore may still prove useful for nanopore sensors because it could be used in conjunction with open pore analysis, which is more ideal for estimating peptide concentrations, to better inform the experimenter that an unknown peptide mixture contains a number of different cysteine-containing peptides. If one uses the clusters in addition to open pore analysis, then it could provide a powerful tool for improving the prospects for cysteine-containing peptide mixture analysis.

Open-pore resistive-pulse analysis is typically used to associate current blockades with a particular molecule. 41,62 For the case of a simple polymer like PEG, this analysis is straightforward because the current blockades are low noise and single leveled. 63 Indeed, peptide analysis with open pores has had success for various homopolymer peptides⁶⁴ and transside analysis.⁶³ However, open pore analysis of peptides is generally more complicated because the peptides give rise to a wide variety of blockade types (short-lived, translocating, and multistate). These complex blockades result from a number of factors (e.g., solubility, secondary structure) that limits the pore's ability to distinguish between peptides. This can be seen from the open pore current traces and corresponding blockade examples of several of the peptides from Table S1 (see Figures S8 and S9 in the Open Pore Peptide Sensing section of the Supporting Information).

One can imagine an experiment where a peptide mixture is introduced to an open pore system. This gives rise to current blockades that may yield overlapping (low resolution) distributions among the different peptides in the mixture. The additional gold cluster data could help identify the presence of multiple cysteine-containing peptides. To illustrate this, we present data in Figure S10 (see the "Comparing Mixture Analysis between Open Pore and the Cluster Protocol" section in the Supporting Information) which shows a combination of open pore and cluster-based analysis of a 7C1 and 9C1 mixture. The open pore data result from ejection of the mixture onto an open αHL pore for an extended period (\approx 20 min). This gives rise to several thousand single molecule blockades whose various characteristics (i.e., blockade depth, duration, and standard deviation) are each distributed in a unimodal fashion (see left panel of Figure S10). This means the open pore is essentially blind to the fact that there are two distinct peptides in the mixture. However, by measuring this same mixture with gold clusters in the pore, we find clear evidence of two distinct current signatures (see right panel of Figure S10). This additional information correctly indicates the presence of two cysteinecontaining peptides in the mixture, which do not appear in the open pore analysis.

Collecting gold cluster data, in parallel with the open pore data, could make it possible to identify the presence of multiple cysteine-containing peptides that may not be distinguishable from the open pore data alone. This information could better inform a machine learning search of peptide mixtures⁶⁵ and shows the potential that our gold cluster protocol could have on the analysis of unknown peptide mixtures.

CONCLUSIONS

Nanopore-bound metallic clusters have shown promise as sensors via ligand exchange and surface attachment processes. Cysteine-containing peptides can be selectively detected, and the corresponding fluctuations can be used to identify each peptide attachment. Here, we have shown the different types of fluctuations that arise with the attachment of various peptides, and these yield either stable transitions between current states where the transition steps are well-correlated with the peptide mass or high-frequency two-state fluctuations. These highfrequency fluctuations were shown to depend on various physical (length, charge) and chemical (sequence) characteristics. We then demonstrated that the peptide-induced fluctuations can be analyzed to identify peptides in mixtures from both the current-step and the high-frequency peptide types. In fact, the distinct nature of the high-frequency fluctuations provides a clear indication of the peptide that attaches at the single peptide limit. We believe this clusterbased approach to peptide sensing could provide a useful means for identifying low-mass cysteine-containing peptides that can play an important role in proteolytic-based peptide and protein sensors.

METHODS

Materials. Nanopore Experiments. 1,2-Diphytanoyl-sn-glycero-3phospholcholine (DPhyPC) lipid was purchased from Avanti Polar Lipids (Alabaster, AL). Teflon sheets were purchased from Goodfellow USA Corp. (Coraopolis, PA). 50 μm diameter holes were formed in the Teflon sheets with laser drilling at Potomac Photonics (Halethrope, MD). Borosilicate glass capillaries, with filament, having an external diameter of 1 mm and internal diameters of 0.5 mm and 0.78 mm were purchased from Sutter Instruments (Novato, CA). The micropipettes for lipid ejection and for analyte ejection were made from the glass capillaries of 0.5 mm and 0.78 mm, respectively, using a P-2000 puller (Sutter Instruments) with preset program #11. Chemicals such as potassium tetrachloroaurate (III) hydrate, Tris (hydroxymethyl) aminomethane (TRIS), tiopronin (TP), potassium chloride (KCl), hexadecane, citric acid, and potassium hydroxide (KOH) were purchased from Sigma-Aldrich (St. Louis, MO). Boranetert-butylamine complex (BTBC) was purchased from Alfa Aesar, (Ward Hill, MA). n-Pentane and methanol were purchased from Fisher Scientific (Washington, DC). Alpha toxin from Staphylococcus aureus was purchased from IBT Bioservices (Rockville, MD).

Peptide Synthesis and Purification. All chemicals and reagents used for peptide purification were purchased from Thermo-Fisher Scientific (Waltham, MA), VWR (Radnor, PA), or Sigma-Aldrich (St. Louis, MO). Table S1 details all peptides used throughout this study.

Methodology. Cluster Synthesis. Water-soluble TP-capped gold clusters were synthesized using a previously established protocol. Solutions of potassium tetrachloroaurate (III) hydrate, TP, and BTBC were created at a concentration of 2.5 mM in methanol and then mixed in a 2:2:1 volumetric ratio, respectively. First, 700 μ L of gold solution was mixed with 700 μ L of TP ligand solution and shaken for several seconds. This was followed by the addition of 350 μ L of BTBC solution. The final mixture was vortexed and sonicated for about 30 min during which time the solution would turn from clear to brown, indicating the formation of nanoclusters. This mixture was then left open in a fume hood for 12–24 h until all methanol

evaporated away and the dried sample was affixed to the inside of the container surface. The dried sample was rehydrated using 1 mL of type I ultrapure water (18.2 M Ω -cm), and the sample was stored at 4 °C and remained stable over a period of 1–2 months. From the values listed here, we estimate the stock nanocluster concentration to be on the order of 20 μ M (assuming an average of 100 gold atoms per cluster).

Peptide Synthesis and Characterization. Peptide variants were synthesized using standard FMOC chemistry in-house as previously described or purchased from GenScript (Piscataway, NJ). Peptides were purified via reversed-phase HPLC Vydac C4 column, eluted by a linear gradient of water:acetonitrile (both supplemented with 0.1% TFA). Peptide identity and purity were confirmed using LC-MS to >95% purity. Peptide concentration was determined using Beer's law with an extinction coefficient of 5680 ${\rm M}^{-1}$ cm $^{-1}$. Each peptide stock for CD analysis was made to a final concentration of 150–200 μM then stored at 4 °C.

Nanopore Sensing and Data Analysis. The nanopore set up and methodology are nearly identical to one previously described.⁵¹ The electrolyte buffer used here was 3 M KCl, 10 mM Tris at pH 8.0. Following the formation of a single αHL channel in an unsupported DPhyPC membrane, we applied a 70 mV transmembrane voltage (Axopatch 200B, Molecular Devices, San Jose, CA), which yielded an easily detectable current through the nanopore. Figure 1A illustrates the principle of operation where two microcapillaries are positioned ca. 50 μ m from the pore-containing membrane, and a backing pressure (~10 hPa) was applied for several seconds with a pump (Femtojet, Eppendorf, Hauppauge, NY) to eject TP-capped clusters into the cis-side of the αHL pore. After the capture of a single TPcapped cluster, the backing pressure was removed from the clustercontaining tip to eliminate the possibility of multiple cluster captures. Following this capture, pressure was applied to a second capillary tip that contained the peptide of interest (~10 s). This caused peptides to be ejected onto the pore-bound cluster, and current was recorded for extended periods during and after the peptide-tip pressure was applied. Unless stated otherwise, peptide concentration in the capillary tip was 500 μ M and the total solution volume in each tip was ca. 5 μ L. The peptide concentration at the pore is greatly reduced due to diffusion effects, and we estimate it to be on the order of 10 µM. Further discussion of this phenomenon can be found elsewhere.⁶⁷ To minimize effects from peptide aggregation at these higher concentrations, peptide solutions were typically discarded after 1 week.

Current signals were digitized and collected at a sampling rate of 50 kHz (Digidata 1550B, Molecular Devices) with a four-pole low-pass Bessel filter set to 10 kHz. Current traces were recorded with pCLAMP 10.7 software (Molecular Devices). Further analysis (i.e., histograms, digital filtering, and multipeak fitting) was performed with IGOR 6.37 (Wavemetrics, Portland, OR). Current signal traces were reported with either the 10 kHz filter or a postprocessed 100 Hz digital filter using IGOR software (4-pole, infinite impulse response filter). An in-house MATLAB-based (MATLAB R2019a, Mathworks, Natick, MA) cumulative sum analyzer was used to analyze current step distributions as needed. Sel All plots were generated using the IGOR software.

Percentage mixture analysis for the low-frequency peptides RGDC and GRGDSPC from Figure 5 was performed as follows. Downward going current steps >4 pA were analyzed for 24 different exchange experiments (237 steps on 24 clusters over 3 different nanopores) and used to construct the step distributions, shown as the black line with empty circles in Figure 5A. This distribution was fit with two Gaussians (one for each peptide) $f(i) = A \exp(-((i - i_0)/w)^2)$. The following parameters were used to fit the distributions: (RGDC): A = 38, $i_0 = -6.75$ pA, w = 1.45 pA and (GRGDSPC): A = 18, $i_0 = -9.7$ pA, w = 0.75 pA. These distributions are represented with the blue (GRGDSPC) and red (RGDC) transparent shaded functions in Figure 5. The sum of the two distributions (solid red line) is the least-squares fit to the experimental distribution. From this fitting, we arrive at functions that yield the probability of a current step (i) resulting from either a RGDC peptide $P_{\rm RGDC}(i) = f_{\rm RGDC}(i)/(f_{\rm RGDC}(i))$

 $f_{\mathrm{GRGDSPC}}(i)$) or a GRGDSPC peptide $P_{\mathrm{GRGDSPC}}(i) = f_{\mathrm{GRGDSPC}}(i)/(f_{\mathrm{RGDC}}(i) + f_{\mathrm{GRGDSPC}}(i))$. These percentages are reported in the Figure 5 caption.

TEM Measurements. The TP-Au nanoparticle images were obtained from a transmission electron microscope (TEM) (JEM-200, JEOL, Peabody, MA) operated at 200 keV and equipped with a cold cathode. Particles were ejected onto a mesh 200 carbon-coated Cu grid. Particle sizes were analyzed with ImageJ software in a manner previously described. ⁶⁸

ASSOCIATED CONTENT

Supporting Information

The Supporting Information is available free of charge at https://pubs.acs.org/doi/10.1021/acsnano.2c07842.

The following sections are contained: Summary of peptides studied, CD spectral analysis of peptides, analysis of TP-capped nanoclusters, cysteine selective detection, summary of high-frequency peptide fluctuations, current step ligand analysis, $P_{\rm left}$ model, open pore peptide sensing, and comparing mixture analysis between open pore and the cluster protocol (PDF)

AUTHOR INFORMATION

Corresponding Author

Joseph E. Reiner — Department of Physics, Virginia Commonwealth University, Richmond, Virginia 23284, United States; orcid.org/0000-0002-1056-8703; Email: jereiner@vcu.edu

Authors

- Madhav L. Ghimire Department of Physics, Virginia Commonwealth University, Richmond, Virginia 23284, United States
- Bobby D. Cox Department of Physics, Virginia Commonwealth University, Richmond, Virginia 23284, United States
- Cole A. Winn Department of Physics, Virginia Commonwealth University, Richmond, Virginia 23284, United States
- Thomas W. Rockett Department of Physics, Virginia Commonwealth University, Richmond, Virginia 23284, United States
- Nicholas P. Schifano Department of Chemistry and Biochemistry, Rowan University, Glassboro, New Jersey 08028, United States
- Hannah M. Slagle Department of Chemistry and Biochemistry, Rowan University, Glassboro, New Jersey 08028, United States
- Frank Gonzalez Department of Chemistry and Biochemistry, Rowan University, Glassboro, New Jersey 08028, United States
- Massimo F. Bertino Department of Physics, Virginia Commonwealth University, Richmond, Virginia 23284, United States; © orcid.org/0000-0001-6029-0685
- Gregory A. Caputo Department of Chemistry and Biochemistry, Rowan University, Glassboro, New Jersey 08028, United States; orcid.org/0000-0002-4510-2815

Complete contact information is available at: https://pubs.acs.org/10.1021/acsnano.2c07842

Funding

This material is based upon work supported by the National Science Foundation under grant CBET-2011173. F.G. was

supported by the National Institutes of Health under grant R25GM119973. Additional funding was provided by the VCU-CHS SEED award.

Notes

The authors declare no competing financial interest.

ACKNOWLEDGMENTS

The TEM imaging was performed at the VCU Nanomaterials Characterization Core (NCC) Facility. We are grateful to Dr. Carl Mayer for his valuable assistance with the TEM imaging. We also acknowledge Dr. Joseph Turner for his valuable assistance with the UV—vis spectroscopy.

REFERENCES

- (1) Boschetti, E.; D'Amato, A.; Candiano, G.; Righetti, P. G. Protein Biomarkers for Early Detection of Diseases: The Decisive Contribution of Combinatorial Peptide Ligand Libraries. *J. Proteomics* **2018**, *188*, 1–14.
- (2) Schulte, I.; Tammen, H.; Selle, H.; Schulz-Knappe, P. Peptides in Body Fluids and Tissues as Markers of Disease. *Expert Rev. Mol. Diagn.* **2005**, *5*, 145–157.
- (3) Wang, X.; Yu, J.; Sreekumar, A.; Varambally, S.; Shen, R.; Giacherio, D.; Mehra, R.; Montie, J. E.; Pienta, K. J.; Sanda, M. G.; Kantoff, P. W.; Rubin, M. A.; Wei, J. T.; Ghosh, D.; Chinnaiyan, A. M. Autoantibody Signatures in Prostate Cancer. N. Engl. J. of Med. 2005, 353, 1224–1235.
- (4) Chakraborty, S.; Andrieux, G.; Hasan, A. M. M.; Ahmed, M.; Hosen, M. I.; Rahman, T.; Hossain, M. A.; Boerries, M. Harnessing the Tissue and Plasma LncRNA-Peptidome to Discover Peptide-Based Cancer Biomarkers. *Sci. Rep.* **2019**, *9*, 12322.
- (5) Frantzi, M.; van Kessel, K. E.; Zwarthoff, E. C.; Marquez, M.; Rava, M.; Malats, N.; Merseburger, A. S.; Katafigiotis, I.; Stravodimos, K.; Mullen, W.; Zoidakis, J.; Makridakis, M.; Pejchinovski, M.; Critselis, E.; Lichtinghagen, R.; Brand, K.; Dakna, M.; Roubelakis, M. G.; Theodorescu, D.; Vlahou, A.; Mischak, H.; Anagnou, N. P. Development and Validation of Urine-Based Peptide Biomarker Panels for Detecting Bladder Cancer in a Multi-Center Study. *Clin. Cancer Res.* 2016, 22, 4077–4086.
- (6) Petricoin, E. F.; Belluco, C.; Araujo, R. P.; Liotta, L. A. The Blood Peptidome: A Higher Dimension of Information Content for Cancer Biomarker Discovery. *Nat. Rev. Cancer* **2006**, *6*, 961–967.
- (7) van den Broek, I.; Sparidans, R. W.; Schellens, J. H. M.; Beijnen, J. H. Quantitative Assay for Six Potential Breast Cancer Biomarker Peptides in Human Serum by Liquid Chromatography Coupled to Tandem Mass Spectrometry. *J. Chromatogr. B* **2010**, *878*, 590–602.
- (8) Cao, Z.; Kamlage, B.; Wagner-Golbs, A.; Maisha, M.; Sun, J.; Schnackenberg, L. K.; Pence, L.; Schmitt, T. C.; Daniels, J. R.; Rogstad, S.; Beger, R. D.; Yu, L.-R. An Integrated Analysis of Metabolites, Peptides, and Inflammation Biomarkers for Assessment of Preanalytical Variability of Human Plasma. *J. Proteome Res.* 2019, 18. 2411–2421.
- (9) Murata, M.; Kawanishi, S. Oxidative DNA Damage Induced by Nitrotyrosine, a Biomarker of Inflammation. *Biochem. Biophys. Res. Commun.* **2004**, *316*, 123–128.
- (10) Piktel, E.; Levental, I.; Durnas, B.; Janmey, P. A.; Bucki, R. Plasma Gelsolin: Indicator of Inflammation and Its Potential as a Diagnostic Tool and Therapeutic Target. *Int. J. Mol. Sci.* **2018**, *19*, 2516.
- (11) Al Shweiki, M. R.; Oeckl, P.; Pachollek, A.; Steinacker, P.; Barschke, P.; Halbgebauer, S.; Anderl-Straub, S.; Lewerenz, J.; Ludolph, A. C.; Bernhard Landwehrmeyer, G.; Otto, M. Cerebrospinal Fluid Levels of Prodynorphin-Derived Peptides Are Decreased in Huntington's Disease. *Mov. Disord.* **2021**, *36*, 492–497.
- (12) Ashton, N. J.; Hye, A.; Rajkumar, A. P.; Leuzy, A.; Snowden, S.; Suárez-Calvet, M.; Karikari, T. K.; Schöll, M.; La Joie, R.; Rabinovici, G. D.; Höglund, K.; Ballard, C.; Hortobágyi, T.; Svenningsson, P.; Blennow, K.; Zetterberg, H.; Aarsland, D. An Update on Blood-Based

- Biomarkers for Non-Alzheimer Neurodegenerative Disorders. *Nat. Rev. Neurol.* **2020**, *16*, 265–284.
- (13) Bibl, M.; Mollenhauer, B.; Lewczuk, P.; Esselmann, H.; Wolf, S.; Trenkwalder, C.; Otto, M.; Stiens, G.; Rüther, E.; Kornhuber, J.; Wiltfang, J. Validation of Amyloid-β Peptides in CSF Diagnosis of Neurodegenerative Dementias. *Mol. Psychiatry* **2007**, *12*, 671–680.
- (14) Blankenberg, S.; McQueen, M. J.; Smieja, M.; Pogue, J.; Balion, C.; Lonn, E.; Rupprecht, H. J.; Bickel, C.; Tiret, L.; Cambien, F.; Gerstein, H.; Münzel, T.; Yusuf, S. Comparative Impact of Multiple Biomarkers and N-Terminal Pro-Brain Natriuretic Peptide in the Context of Conventional Risk Factors for the Prediction of Recurrent Cardiovascular Events in the Heart Outcomes Prevention Evaluation (HOPE) Study. *Circulation* **2006**, *114*, 201–208.
- (15) Braunwald, E. Biomarkers in Heart Failure. N. Engl. J. of Med. **2008**, 358, 2148–2159.
- (16) Magnussen, C.; Blankenberg, S. Biomarkers for Heart Failure: Small Molecules with High Clinical Relevance. *J. Int. Med.* **2018**, 283, 530–543.
- (17) Broza, Y. Y.; Zhou, X.; Yuan, M.; Qu, D.; Zheng, Y.; Vishinkin, R.; Khatib, M.; Wu, W.; Haick, H. Disease Detection with Molecular Biomarkers: From Chemistry of Body Fluids to Nature-Inspired Chemical Sensors. *Chem. Rev.* **2019**, *119*, 11761–11817.
- (18) Machera, S. J.; Niedziółka-Jönsson, J.; Szot-Karpińska, K. Phage-Based Sensors in Medicine: A Review. *Chemosensors* **2020**, 8, 61.
- (19) Smith, C. R.; Batruch, I.; Bauça, J. M.; Kosanam, H.; Ridley, J.; Bernardini, M. Q.; Leung, F.; Diamandis, E. P.; Kulasingam, V. Deciphering the Peptidome of Urine from Ovarian Cancer Patients and Healthy Controls. *Clin. Proteom.* **2014**, *11*, 23.
- (20) Begcevic, I.; Brinc, D.; Brown, M.; Martinez-Morillo, E.; Goldhardt, O.; Grimmer, T.; Magdolen, V.; Batruch, I.; Diamandis, E. P. Brain-Related Proteins as Potential CSF Biomarkers of Alzheimer's Disease: A Targeted Mass Spectrometry Approach. *J. Proteomics* **2018**, 182, 12–20.
- (21) Demirev, P. A.; Fenselau, C. Mass Spectrometry in Biodefense. *J. Mass Spectrom.* **2008**, *43*, 1441–1457.
- (22) Macklin, A.; Khan, S.; Kislinger, T. Recent Advances in Mass Spectrometry Based Clinical Proteomics: Applications to Cancer Research. *Clin. Proteom.* **2020**, *17*, 17.
- (23) Fricker, L. D. Limitations of Mass Spectrometry-Based Peptidomic Approaches. *J. Am. Soc. Mass Spectrom.* **2015**, 26, 1981–1991.
- (24) Dai, J.; Wang, J.; Zhang, Y.; Lu, Z.; Yang, B.; Li, X.; Cai, Y.; Qian, X. Enrichment and Identification of Cysteine-Containing Peptides from Tryptic Digests of Performic Oxidized Proteins by Strong Cation Exchange LC and MALDI-TOF/TOF MS. *Anal. Chem.* 2005, 77, 7594–7604.
- (25) Eitner, K.; Koch, U.; Gawęda, T.; Marciniak, J. Statistical Distribution of Amino Acid Sequences: A Proof of Darwinian Evolution. *Bioinformatics* **2010**, *26*, 2933–2935.
- (26) Anfossi, L.; Baggiani, C.; Giovannoli, C.; D'Arco, G.; Giraudi, G. Lateral-Flow Immunoassays for Mycotoxins and Phycotoxins: A Review. *Anal. Bioanal. Chem.* **2013**, 405, 467–480.
- (27) Clerico, A.; Del Ry, S.; Giannessi, D. Measurement of Cardiac Natriuretic Hormones (Atrial Natriuretic Peptide, Brain Natriuretic Peptide, and Related Peptides) in Clinical Practice: The Need for a New Generation of Immunoassay Methods. *Clin. Chem.* **2000**, *46*, 1529–1534.
- (28) Hage, D. S. Immunoassays. Anal. Chem. 1999, 71, 294-304.
- (29) Hassanpour, S.; Hasanzadeh, M. Label-Free Electrochemical-Immunoassay of Cancer Biomarkers: Recent Progress and Challenges in the Efficient Diagnosis of Cancer Employing Electroanalysis and Based on Point of Care (POC). *Microchem. J.* **2021**, *168*, 106424.
- (30) Li, Y.; Zhang, G.; Mao, X.; Yang, S.; De Ruyck, K.; Wu, Y. High Sensitivity Immunoassays for Small Molecule Compounds Detection Novel Noncompetitive Immunoassay Designs. *Trends Anal. Chem.* **2018**, *103*, 198–208.

- (31) Becker, J. O.; Hoofnagle, A. N. Replacing Immunoassays with Tryptic Digestion-Peptide Immunoaffinity Enrichment and LC-MS/MS. *Bioanalysis* **2012**, *4*, 281–290.
- (32) Hoofnagle, A. N.; Wener, M. H. The Fundamental Flaws of Immunoassays and Potential Solutions Using Tandem Mass Spectrometry. J. Immunol. Methods 2009, 347, 3–11.
- (33) Chang, P.-H.; Weng, C.-C.; Li, B.-R.; Li, Y.-K. An Antifouling Peptide-Based Biosensor for Determination of Streptococcus Pneumonia Markers in Human Serum. *Biosens. Bioelectron.* **2020**, *151*, 111969.
- (34) Karimzadeh, A.; Hasanzadeh, M.; Shadjou, N.; Guardia, M. de la. Peptide Based Biosensors. *Trends Anal. Chem.* **2018**, *107*, 1–20.
- (35) Liu, Q.; Wang, J.; Boyd, B. J. Peptide-Based Biosensors. *Talanta* **2015**, 136, 114–127.
- (36) Tian, L.; Heyduk, T. Antigen Peptide-Based Immunosensors for Rapid Detection of Antibodies and Antigens. *Anal. Chem.* **2009**, *81*, 5218–5225.
- (37) Vanova, V.; Mitrevska, K.; Milosavljevic, V.; Hynek, D.; Richtera, L.; Adam, V. Peptide-Based Electrochemical Biosensors Utilized for Protein Detection. *Biosens. Bioelectron.* **2021**, *180*, 113087.
- (38) Kasianowicz, J. J.; Robertson, J. W. F.; Chan, E. R.; Reiner, J. E.; Stanford, V. M. Nanoscopic Porous Sensors. *Annu. Rev. Anal. Chem.* **2008**, *1*, 737–766.
- (39) Neuman, K. C.; Nagy, A. Single-Molecule Force Spectroscopy: Optical Tweezers, Magnetic Tweezers and Atomic Force Microscopy. *Nat. Methods* **2008**, *5*, 491–505.
- (40) Zhao, Y.; Ashcroft, B.; Zhang, P.; Liu, H.; Sen, S.; Song, W.; Im, J.; Gyarfas, B.; Manna, S.; Biswas, S.; Borges, C.; Lindsay, S. Single-Molecule Spectroscopy of Amino Acids and Peptides by Recognition Tunnelling. *Nat. Nanotechnol.* **2014**, *9*, 466–473.
- (41) Robertson, J. W. F.; Ghimire, M. L.; Reiner, J. E. Nanopore Sensing: A Physical-Chemical Approach. *Biochimica et Biophysica Acta* (BBA) Biomembranes **2021**, 1863, 183644.
- (42) Brinkerhoff, H.; Kang, A. S. W.; Liu, J.; Aksimentiev, A.; Dekker, C. Multiple Rereads of Single Proteins at Single-Amino Acid Resolution Using Nanopores. *Science* **2021**, *374*, 1509–1513.
- (43) Alfaro, J. A.; Bohländer, P.; Dai, M.; Filius, M.; Howard, C. J.; van Kooten, X. F.; Ohayon, S.; Pomorski, A.; Schmid, S.; Aksimentiev, A.; Anslyn, E. V.; Bedran, G.; Cao, C.; Chinappi, M.; Coyaud, E.; Dekker, C.; Dittmar, G.; Drachman, N.; Eelkema, R.; Goodlett, D.; Hentz, S.; Kalathiya, U.; Kelleher, N. L.; Kelly, R. T.; Kelman, Z.; Kim, S. H.; Kuster, B.; Rodriguez-Larrea, D.; Lindsay, S.; Maglia, G.; Marcotte, E. M.; Marino, J. P.; Masselon, C.; Mayer, M.; Samaras, P.; Sarthak, K.; Sepiashvili, L.; Stein, D.; Wanunu, M.; Wilhelm, M.; Yin, P.; Meller, A.; Joo, C. The Emerging Landscape of Single-Molecule Protein Sequencing Technologies. *Nat. Methods* **2021**, *18*, 604–617. (44) Yan, S.; Zhang, J.; Wang, Y.; Guo, W.; Zhang, S.; Liu, Y.; Cao,
- J.; Wang, Y.; Wang, L.; Ma, F.; Zhang, P.; Chen, H.-Y.; Huang, S. Single Molecule Ratcheting Motion of Peptides in a Mycobacterium Smegmatis Porin A (MspA) Nanopore. *Nano Lett.* **2021**, 21, 6703–6710.
- (45) Zhang, S.; Huang, G.; Versloot, R. C. A.; Bruininks, B. M. H.; de Souza, P. C. T.; Marrink, S.-J.; Maglia, G. Bottom-up Fabrication of a Proteasome-Nanopore That Unravels and Processes Single Proteins. *Nat. Chem.* **2021**, *13*, 1192–1199.
- (46) Huo, M.-Z.; Hu, Z.-L.; Ying, Y.-L.; Long, Y.-T. Enhanced Identification of Tau Acetylation and Phosphorylation with an Engineered Aerolysin Nanopore. *Proteomics* **2022**, 22, 2100041.
- (47) Versloot, R. C. A.; Lucas, F. L. R.; Yakovlieva, L.; Tadema, M. J.; Zhang, Y.; Wood, T. M.; Martin, N. I.; Marrink, S. J.; Walvoort, M. T. C.; Maglia, G. Quantification of Protein Glycosylation Using Nanopores. *Nano Lett.* **2022**, *22*, 5357–5364.
- (48) Afshar Bakshloo, M.; Kasianowicz, J. J.; Pastoriza-Gallego, M.; Mathé, J.; Daniel, R.; Piguet, F.; Oukhaled, A. Nanopore-Based Protein Identification. *J. Am. Chem. Soc.* **2022**, *144*, 2716–2725.
- (49) Robertson, J. W. F.; Reiner, J. E. The Utility of Nanopore Technology for Protein and Peptide Sensing. *Proteomics* **2018**, *18*, 1800026.

- (50) Schmid, S.; Stömmer, P.; Dietz, H.; Dekker, C. Nanopore Electro-Osmotic Trap for the Label-Free Study of Single Proteins and Their Conformations. *Nat. Nanotechnol.* **2021**, *16*, 1244–1250.
- (51) Cox, B. D.; Ghimire, M. L.; Bertino, M. F.; Reiner, J. E. Resistive-Pulse Nanopore Sensing of Ligand Exchange at the Single Nanocluster Limit for Peptide Detection. *ACS Appl. Nano Mater.* **2020**, *3*, 7973–7981.
- (52) Fahie, M. A.; Chen, M. Electrostatic Interactions between OmpG Nanopore and Analyte Protein Surface Can Distinguish between Glycosylated Isoforms. *J. Phys. Chem. B* **2015**, *119*, 10198–10206
- (53) Nivala, J.; Mulroney, L.; Li, G.; Schreiber, J.; Akeson, M. Discrimination among Protein Variants Using an Unfoldase-Coupled Nanopore. *ACS Nano* **2014**, *8*, 12365–12375.
- (54) Rostovtseva, T. K.; Gurnev, P. A.; Hoogerheide, D. P.; Rovini, A.; Sirajuddin, M.; Bezrukov, S. M. Sequence Diversity of Tubulin Isotypes in Regulation of the Mitochondrial Voltage-Dependent Anion Channel. *J. Biol. Chem.* **2018**, 293, 10949–10962.
- (55) Xie, H.; Braha, O.; Gu, L.-Q.; Cheley, S.; Bayley, H. Single-Molecule Observation of the Catalytic Subunit of CAMP-Dependent Protein Kinase Binding to an Inhibitor Peptide. *Chem. Biol.* **2005**, *12*, 109–120.
- (56) Cox, B. D.; Woodworth, P. H.; Wilkerson, P. D.; Bertino, M. F.; Reiner, J. E. Ligand-Induced Structural Changes of Thiolate-Capped Gold Nanoclusters Observed with Resistive-Pulse Nanopore Sensing. *J. Am. Chem. Soc.* **2019**, *141*, 3792–3796.
- (57) Cox, B. D.; Martin, C. R.; Bertino, M. F.; Reiner, J. E. Biological Nanopores Elucidate the Differences between Isomers of Mercaptobenzoic-Capped Gold Clusters. *Phys. Chem. Chem. Phys.* **2021**, 23, 7938–7947.
- (58) Giesbers, M.; Kleijn, J. M.; Cohen Stuart, M. A. Interactions between Acid- and Base-Functionalized Surfaces. *J. Colloid Interface Sci.* **2002**, 252, 138–148.
- (59) Carugo, O. Amino Acid Composition and Protein Dimension. *Protein Sci.* **2008**, *17*, 2187–2191.
- (60) Lucas, F. L. R.; Versloot, R. C. A.; Yakovlieva, L.; Walvoort, M. T. C.; Maglia, G. Protein Identification by Nanopore Peptide Profiling. *Nat. Commun.* **2021**, *12*, 5795.
- (61) Fu, J.; Wu, L.; Qiao, Y.; Tu, J.; Lu, Z. Microfluidic Systems Applied in Solid-State Nanopore Sensors. *Micromachines* **2020**, *11*, 332.
- (62) Reiner, J. E.; Balijepalli, A.; Robertson, J. W. F.; Campbell, J.; Suehle, J.; Kasianowicz, J. J. Disease Detection and Management via Single Nanopore-Based Sensors. *Chem. Rev.* **2012**, *112*, 6431–6451.
- (63) Chavis, A. E.; Brady, K. T.; Hatmaker, G. A.; Angevine, C. E.; Kothalawala, N.; Dass, A.; Robertson, J. W. F.; Reiner, J. E. Single Molecule Nanopore Spectrometry for Peptide Detection. *ACS Sens.* **2017**, *2*, 1319–1328.
- (64) Piguet, F.; Ouldali, H.; Pastoriza-Gallego, M.; Manivet, P.; Pelta, J.; Oukhaled, A. Identification of Single Amino Acid Differences in Uniformly Charged Homopolymeric Peptides with Aerolysin Nanopore. *Nat. Commun.* **2018**, *9*, 966.
- (65) Wan, Y. K.; Hendra, C.; Pratanwanich, P. N.; Göke, J. Beyond Sequencing: Machine Learning Algorithms Extract Biology Hidden in Nanopore Signal Data. *Trends Genet.* **2022**, *38*, 246–257.
- (66) Kohn, E. M.; Shirley, D. J.; Arotsky, L.; Picciano, A. M.; Ridgway, Z.; Urban, M. W.; Carone, B. R.; Caputo, G. A. Role of Cationic Side Chains in the Antimicrobial Activity of C18G. *Molecules* **2018**, 23, 329.
- (67) Ghimire, M. L.; Gibbs, D. R.; Mahmoud, R.; Dhakal, S.; Reiner, J. E. Nanopore Analysis as a Tool for Studying Rapid Holliday Junction Dynamics and Analyte Binding. *Anal. Chem.* **2022**, *94*, 10027–10034.
- (68) Schneider, C. A.; Rasband, W. S.; Eliceiri, K. W. NIH Image to ImageJ: 25 Years of Image Analysis. *Nat. Methods* **2012**, *9*, 671–675.

□ Recommended by ACS

Cell-Free Expression of $\ensuremath{\textit{De Novo}}$ Designed Peptides That Form β -Barrel Nanopores

Shoko Fujita, Ryuji Kawano, et al.

FEBRUARY 02, 2023

ACS NANO

READ 🗹

Spacer Matters: All-Peptide-Based Ligand for Promoting Interfacial Proteolysis and Plasmonic Coupling

Zhicheng Jin, Jesse V. Jokerst, et al.

NOVEMBER 08, 2022

NANO LETTERS

READ 🗹

β-Barrel Nanopores with an Acidic–Aromatic Sensing Region Identify Proteinogenic Peptides at Low pH

Roderick Corstiaan Abraham Versloot, Giovanni Maglia, et al.

MARCH 18, 2022

ACS NANO

READ 🗹

Cell-Selective Multifunctional Surface Covalent Reconfiguration Using Aptamer-Enabled Proximity Catalytic Labeling

Yuna Guo, Huangxian Ju, et al.

FEBRUARY 23, 2023

JOURNAL OF THE AMERICAN CHEMICAL SOCIETY

READ 🗹

Get More Suggestions >